

Role of spontaneously generated coherence (SGC) in laser cooling of atoms

Rajnandan Choudhury Das, Samir Khan, Thilagaraj R, and Kanhaiya Pandey*

Department of Physics, Indian Institute of Technology Guwahati, Guwahati, Assam 781039, India

(Dated: February 7, 2024)

The well-known sub-Doppler polarization gradient cooling in type-I transition ($F_e = F_g + 1$) is caused by red-detuned lasers. On the other hand, in type-II transition ($F_e \leq F_g$), sub-Doppler cooling takes place through blue-detuned lasers. This opposite behavior for the two types of transitions is due to SGC. In the absence of SGC, both types of transitions show blue-detuned cooling. In this work, we experimentally and theoretically demonstrate blue-detuned cooling for both types of transitions in ^{87}Rb . For completeness, we compare the temperatures in various configurations.

I. INTRODUCTION

Spontaneously generated coherence (SGC) plays an important role in spectroscopy and has been extensively studied in multilevel systems [1–8]. Since the behaviour of laser cooling has a direct connection with the atomic spectrum profile, SGC also plays a crucial role.

In alkali atoms, laser cooling is generally realized using type-I transition, i.e., $F_g \rightarrow F_e = F_g + 1$ (where F_g and F_e are ground and excited state angular momentum). In type-I transition, both Doppler and sub-Doppler cooling require red-detuned lasers. In contrast, for type-II transition ($F_g \geq F_e$), Doppler cooling requires red-detuned lasers, while sub-Doppler cooling requires blue-detuned lasers [9]. The opposite behavior of these two types of transitions is attributed to SGC. Red-detuned sub-Doppler cooling is due to SGC which is prominent if the magnetic sub-levels are degenerate and is therefore fragile to the magnetic field [9–14]. Achieving low temperatures involves carefully nullifying the magnetic field, a task not feasible in the MOT phase. It is known that blue-detuned cooling occurs in MOT at type-II transition and has been demonstrated in Rb with significant advantages [14–16]. Blue-detuned MOTs have also been demonstrated in molecules and are crucial for cold molecule experiments [17–20]. In this work, we show that blue-detuned cooling in MOT is possible even in type-I transition.

In the experiment, we utilize a narrow open transition in ^{87}Rb for MOT [21–23], similar to Li [24, 25], K [26], Ca [27, 28], Sr [29, 30], Yb [31, 32], Dy [33, 34], Er [35–37], Cd [38], Eu [39], etc. The MOT for ^{87}Rb atoms is realized at a narrow open transition at 420 nm, which has a 4-5 times lower theoretical Doppler temperature (33 μK) than the regularly used broad transition at 780 nm. Since the blue transition is open, we observe that the repumper laser plays a crucial role in lowering the temperature of the narrow-line MOT. We observed that the blue-detuned repumper causes further cooling in both type-I ($F_g = 1 \rightarrow F_e = 2$) and type-II ($F_g = 1 \rightarrow F_e = 1$) transitions in the MOT. We have also explored various other configurations that produce both red-detuned and blue-detuned blue MOTs of Rb.

In this work, we undertake a comprehensive numerical investigation employing a density matrix analysis to explore the impact of SGC on the sub-Doppler force within an atomic system characterized by the $F_g = 1 \rightarrow F_e = 2$ transition. Our primary objective is to assess the feasibility of blue detuned laser cooling in MOT. Subsequently, through experimental exploration, we investigate various configurations of blue-detuned MOTs for Rb at a narrow transition on the D_1 and D_2 lines. Our results, augmented by the density matrix analysis, demonstrate the efficacy of blue-detuned laser cooling even in type-I MOTs, achieving sub-Doppler temperatures as low as 24 μK in the D_1 MOT and 31 μK in the D_2 MOT.

II. THEORY

First, we analyze the cooling by two counter-propagating lasers with σ^+ and σ^- polarizations for $F_g = 1 \rightarrow F_e = 2$ with all the magnetic sub-levels (as shown in Fig. 1 (a)) using density matrix calculations. The Hamiltonian, H of the 8 level system under the electric-dipole and rotating wave approximation and in the rotating frame is expressed as: $H = H_A + H_I$, where

$$\begin{aligned} H_A = & 2kv|3\rangle\langle 3| + (kv - \Delta)|4\rangle\langle 4| + (kv - \Delta)|5\rangle\langle 5| \\ & - (kv + \Delta)|6\rangle\langle 6| - (kv + \Delta)|7\rangle\langle 7| \\ & - (3kv + \Delta)|8\rangle\langle 8| \end{aligned} \quad (1)$$

and

$$\begin{aligned} H_I = & \frac{1}{2}\hbar\Omega\{|1\rangle\langle 4| + \frac{1}{\sqrt{6}}|1\rangle\langle 6| + \frac{1}{\sqrt{2}}|2\rangle\langle 5| + \frac{1}{\sqrt{2}}|2\rangle\langle 7| \\ & + \frac{1}{\sqrt{6}}|3\rangle\langle 5| + |3\rangle\langle 8|\} + h.c. \end{aligned} \quad (2)$$

Here, Δ , Ω and k denote the detuning, rabi frequency and the magnitude of the wave-vector of the lasers respectively, v is the velocity of the atoms. The atom-field interaction is described by writing the Liouville-von Neumann equation for the density matrix,

$$\dot{\rho} = -\frac{i}{\hbar}[H, \rho] + L(\rho) \quad (3)$$

Here, $L(\rho)$ accounts for the spontaneous decay of atoms via various channels. 64 simultaneous differential equations are obtained. Only equations for $\dot{\rho}_{12}$, $\dot{\rho}_{13}$ and $\dot{\rho}_{23}$

* kanhaiyapandey@iitg.ac.in

have the effect of SGC, which are given below. The terms appearing due to SGC are underlined>.

$$\dot{\rho}_{12} = -\frac{i}{2}\Omega(\rho_{42} + \frac{1}{\sqrt{6}}\rho_{62}) + \frac{i}{2\sqrt{2}}\Omega^*(\rho_{15} + \rho_{17}) + \Gamma(\frac{1}{\sqrt{2}}\rho_{45} + \frac{1}{\sqrt{3}}\rho_{56} + \frac{1}{2\sqrt{3}}\rho_{67}) \quad (4)$$

$$\dot{\rho}_{13} = -\frac{i}{2}\Omega(\rho_{43} + \frac{1}{\sqrt{6}}\rho_{63}) + \frac{i}{2}\Omega^*(\frac{1}{\sqrt{6}}\rho_{16} + \rho_{18}) + 2ikv\rho_{13} + \Gamma(\frac{1}{\sqrt{6}}\rho_{46} + \frac{1}{2}\rho_{57} + \frac{1}{\sqrt{6}}\rho_{68}) \quad (5)$$

$$\dot{\rho}_{23} = -\frac{i}{2\sqrt{2}}\Omega(\rho_{53} + \rho_{73}) + \frac{i}{2}\Omega^*(\frac{1}{\sqrt{6}}\rho_{26} + \rho_{28}) + ikv\rho_{23} + \Gamma(\frac{1}{2\sqrt{3}}\rho_{56} + \frac{1}{\sqrt{3}}\rho_{67} + \frac{1}{\sqrt{2}}\rho_{78}) \quad (6)$$

The remaining equations are presented in A 1. They are numerically solved and the force experienced by the atom is evaluated from the absorption of the σ^+ and σ^- light, following a similar approach as in [23, 40, 41]. The force on atom can be given by following expression,

$$F_{\text{damp}} = \hbar k \Omega \text{Im}[(\rho_{14} - \rho_{38}) + \frac{1}{\sqrt{2}}(\rho_{25} - \rho_{27}) + \frac{1}{\sqrt{6}}(\rho_{36} - \rho_{16})] \quad (7)$$

In Fig. 1 (b), we present the force vs velocity plot for a large velocity range under the influence of blue detuned lasers. The red dashed (blue solid) curve corresponds to the force in the presence (absence) of SGC. Both the curves reveal indistinguishable Doppler force profiles for large velocity ranges. The analysis indicates that atoms with positive (negative) velocities encounter positive (negative) forces, leading to heating in the presence of blue detuned lasers. This force vs velocity curves undergo sign reversal for negative detuning, indicative of the well known Doppler cooling.

Zooming into the grey-circled region in Fig. 1 (b), Fig. 1 (c) provides a closer examination of the small velocity range. SGC exerts a substantial influence on the force vs velocity behavior, particularly for lower velocities. In the presence of SGC, atoms with positive (negative) velocities experience a more pronounced positive (negative) force compared to the Doppler force alone, contributing to enhanced heating. Conversely, diminishing the impact of SGC results in a sign reversal in the slope of the force vs velocity curve, indicating the onset of blue-detuned cooling in a type-I system. These curves for force vs velocity flip signs for negative detuning, leading to polarization gradient cooling (heating) in the presence (absence) of SGC.

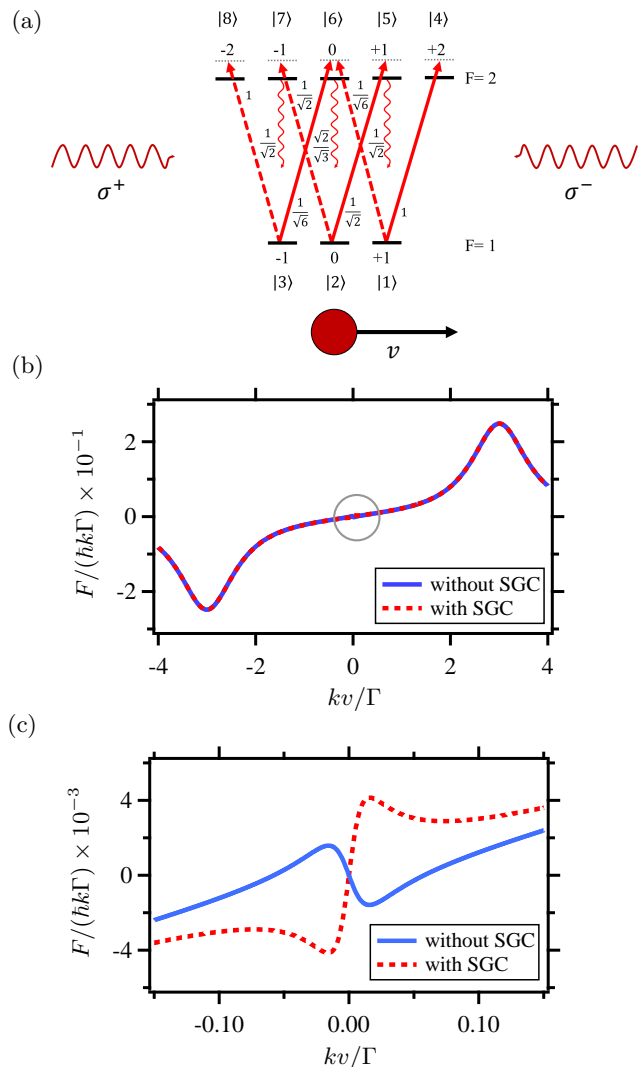


FIG. 1. (Color online) (a) Energy level diagram of the $F_g = 1 \rightarrow F_e = 2$ atomic system. All the Zeeman energy levels are labelled using $|i\rangle$ notation. Clebsch–Gordan coefficients are shown near the transitions. Velocity-dependent force curve for the $F_g = 1 \rightarrow F_e = 2$ system is presented for (b) a large velocity range and (c) a small velocity range. The dashed red (solid blue) curve corresponds to the presence (absence) of SGC. The grey-circled portion in (b) is magnified and illustrated in (c). Parameters: $\Delta_{1 \rightarrow 2} = +3\Gamma$ and $\Omega = \Gamma/\sqrt{2}$.

III. EXPERIMENTAL SETUP

The experimental set-up comprises of one commercially available (Toptica) 420 nm (blue) external cavity diode laser (ECDL) and two home-assembled 780 nm (IR) ECDLs. Polarization spectroscopy is employed for the IR MOT laser's frequency stabilization [21], while saturation absorption spectroscopy is used for the IR repumper laser and the blue laser (similar to our previous experiments [23, 42]). Four sets of beams L_1 , L_2 , L_3 and L_4 are derived which are IR MOT ($5S_{1/2}$, $F = 2 \rightarrow 5P_{3/2}$,

$F = 3$), IR repumper ($5S_{1/2}, F = 1 \rightarrow 5P_{3/2}, F = 1$ or 2), red detuned blue MOT ($5S_{1/2}, F = 2 \rightarrow 6P_{3/2}, F = 3$) and blue detuned blue MOT (at D_1 or D_2 line depending on the configuration) beams respectively. All these beams are switched on/off using AOMs. Each beam is further divided into 3 beams, overlapped, co-propagated, made circularly polarized using dual $\lambda/4$ wave plates, expanded to diameter of 25 mm, sent to the MOT chamber and retro-reflected back using dual $\lambda/4$ wave plate and mirror. In each arm, polarization of L_1 and L_3 are same and L_2 and L_4 are same but orthogonal to L_1 and L_3 .

Atomic vapor is introduced into the MOT chamber by passing 2.15 A current to the dispenser (AlfaSource AS-Rb-0090-2C). First, the IR MOT is loaded for 2 s at quadruple magnetic field (B') of 12.5 G/cm by switching on L_1 (power, 50 mW and detuning -10 MHz from $5S_{1/2}, F = 2 \rightarrow 5P_{3/2}, F = 3$ transition) and L_2 (power, $P_{1 \rightarrow 2} = 33$ mW and detuning, $\Delta_{1 \rightarrow 2}/2\pi = +40$ MHz from $5S_{1/2}, F = 1 \rightarrow 5P_{3/2}, F = 2$) transition. Power of the L_1 is lowered by 5 times and is waited for 4 ms to lower the temperature. Number of atoms, N in the IR MOT is $\sim 1.3 \times 10^8$ and the temperature, T is ~ 2 mK. Then it is transferred to the red detuned blue MOT by switching off the L_1 beam and switching on the L_3 beam (power 26 mW and detuning -7 MHz from $5S_{1/2}, F = 2 \rightarrow 6P_{3/2}, F = 3$ transition). After 4 ms, power of L_3 beam is reduced to 10 mW and detuning is ramped to $\Delta_{2 \rightarrow 3}/2\pi = -3$ MHz in 5 ms. After 20 ms of hold time, L_2, L_3 and B' are switched off. N and T are measured from the time of flight (TOF) method using absorption imaging at $5S_{1/2}, F = 2 \rightarrow 5P_{3/2}, F = 3$ transition on CMOS camera with exposure time of 100 μ s.

IV. RESULTS AND DISCUSSION

We first study the effect of the orthogonally polarized IR repumper laser ($F_g = 1 \rightarrow F_e = 2$) on the IR MOT by changing the power ($P_{1 \rightarrow 2}$) at $\Delta_{1 \rightarrow 2}/2\pi = +40$ MHz. We observe that with increase in $P_{1 \rightarrow 2}$ from 0.5 mW to 33 mW, T of the IR MOT increases from 1 mK to 2 mK. N also increases and saturates to 1.3×10^8 . We then vary $\Delta_{1 \rightarrow 2}/2\pi$ from -20 MHz to $+40$ MHz at $P_{1 \rightarrow 2} = 33$ mW. We observe no significant change in N and T . This is because the IR MOT laser is driving a close transition and only small fraction of atoms are lost due to off-resonant excitation.

Now, we study the effect of IR repumper on the red detuned blue MOT. As the blue transition is open with poor branching ratio, atoms decay continuously to the lower ground state, $F_g=1$. Fig. 2 (b) and (c) show the variation of the T with $P_{1 \rightarrow 2}$ and $\Delta_{1 \rightarrow 2}/2\pi$ respectively for the configuration shown in 2 (a). Here, the L_3 is at -3 MHz detuned to the $5S_{1/2}, F = 2 \rightarrow 6P_{3/2}, F = 3$ transition. First, the repumper laser is kept at $+40$ MHz detuned to the $F = 1 \rightarrow F = 2$ transition (which is also a type-I transition) and the power of the repumper laser is varied. We observe that with increase in $P_{1 \rightarrow 2}$ from

5 mW to 30 mW, T decreases from 80 μ K to 65 μ K as shown in Fig. 2 (b) by filled blue circle points. This is opposite to the case when the repumper laser is red detuned. When $\Delta_{1 \rightarrow 2}/2\pi = -5$ MHz, T increases from 90 μ K to 105 μ K as shown by unfilled red circle points (a). In both the cases, N increases with the increase in $P_{1 \rightarrow 2}$ and then saturates to 1.1×10^8 .

Next, we study the behavior of the red detuned blue MOT with the detuning of the repumper laser, $\Delta_{1 \rightarrow 2}/2\pi$ at three different power: 10 mW, 20 mW and 33 mW, as shown in Fig. 2 (c) by unfilled green diamond, filled yellow triangle and filled blue circle points respectively. When $\Delta_{1 \rightarrow 2}/2\pi$ is varied from -20 MHz to $+40$ MHz at $P_{1 \rightarrow 2} = 33$ mW, T decreases from 120 μ K to 75 μ K and then saturates. Similar pattern is observed at $P_{1 \rightarrow 2} = 10$ mW and 20 mW. We observe that blue detuned laser cooling works even at type-I transition and the blue detuned repumper laser help the narrow line MOT at blue transition to reach lower temperature than the red detuned repumper laser.

Same study is done for the configuration shown in Fig. 3 (a), where the repumper laser is -5.2 MHz red detuned to the $F = 1 \rightarrow F = 1$ transition, which is a type-II transition. Similar to the previous case, T increases from 120 μ K to 150 μ K when the power of the repumper laser ($P_{1 \rightarrow 1}$) is increased from 5 mW to 30 mW (as shown in red in Fig. 3 (b)). In the blue detuned repumper laser configuration i.e. when $\Delta_{1 \rightarrow 1}/2\pi = +17.4$ MHz, T shows a decreasing trend from 90 μ K to 44 μ K with increase in $P_{1 \rightarrow 1}$ from 5 mW to 30 mW. In both the cases, N increases with $P_{1 \rightarrow 1}$ and then saturates to 1.1×10^8 .

We study the effect of repumper laser detuning ($\Delta_{1 \rightarrow 1}$) on the blue MOT at three different powers: 10 mW, 20 mW and 31.5 mW (as shown in Fig. 3 (b) by unfilled green diamond, filled yellow triangle and filled blue circle points respectively). At $P_{1 \rightarrow 1} = 31.5$ mW, T decreases from > 200 μ K to 44 μ K and reaches saturation as the $\Delta_{1 \rightarrow 1}/2\pi$ is changed from -10 MHz to $+17$ MHz. Similar trend is observed when $P_{1 \rightarrow 1} = 10$ mW and 20 mW, but T saturates to higher value.

Next, we demonstrate the red detuned blue MOT using $5S_{1/2}, F = 2 \rightarrow 6P_{3/2}, F = 2$ transition (type-II MOT) with repumper laser at 30 mW and $+14$ MHz blue detuned from the $5S_{1/2}, F = 1 \rightarrow 5P_{3/2}, F = 1$ transition. We study the effect of the power ($P_{2 \rightarrow 2}$) of the red detuned blue MOT beam at $\Delta_{2 \rightarrow 2}/2\pi = -2.5$ MHz and observe that with increase in $P_{2 \rightarrow 2}$ from 5 mW to 20 mW, T decreases from 60 μ K to 32 μ K and then increases after 20 mW, as show in Fig. 4 (b). Then we study the effect of $\Delta_{2 \rightarrow 2}$ on the blue MOT at $P_{2 \rightarrow 2} = 26$ mW and observe that T initially decreases from 38 μ K to 32 μ K as the $\Delta_{2 \rightarrow 2}/2\pi$ is changed from -4 MHz to -2.5 MHz and then increases to > 40 μ K as the detuning is changed towards zero (as shown in Fig. 4 (c)). As compared to the minimum temperature of the red detuned blue MOT at $5S_{1/2}, F = 2 \rightarrow 6P_{3/2}, F = 3$ transition (44 μ K), T of the red detuned blue MOT at $5S_{1/2}, F = 2 \rightarrow 6P_{3/2}, F = 2$ transition (32 μ K) is lower.

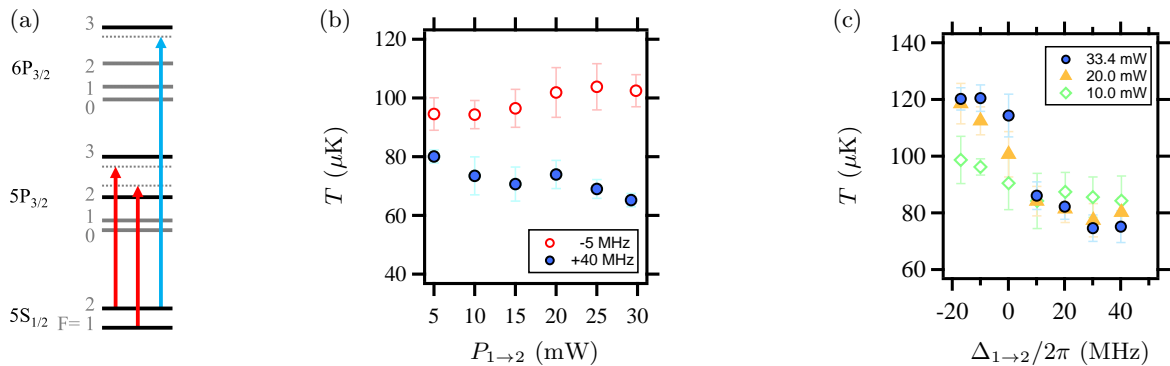


FIG. 2. (Color online) (a) Relevant energy levels for studying the effect of repumper laser addressing $F = 1 \rightarrow 2$ transition. (b) Temperature vs power of the repumper laser when $\Delta_{1 \rightarrow 2}/2\pi = +40$ MHz (filled blue circle) and -5 MHz (unfilled red circle). (c) Temperature vs detuning of the repumper laser when $P_{1 \rightarrow 2} = 10$ mW (unfilled green diamond), 20 mW (filled yellow triangle) and 33.4 mW (filled blue circle).

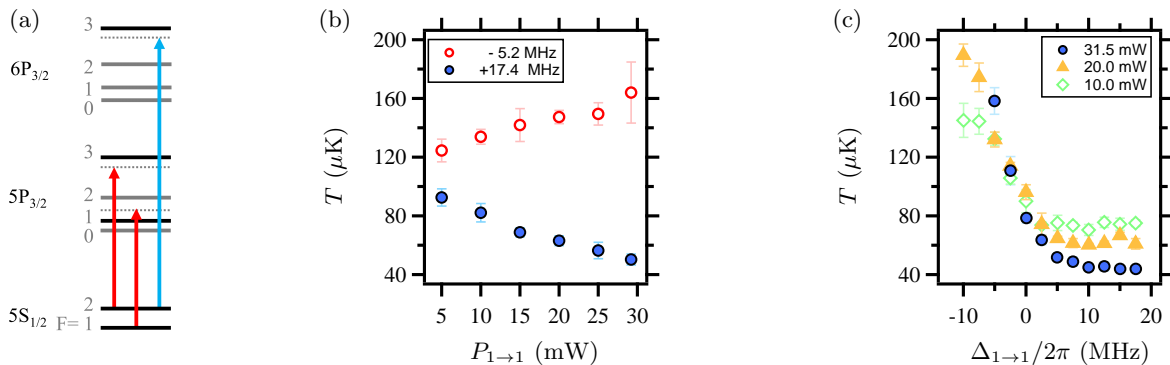


FIG. 3. (Color online) (a) Relevant energy levels for studying the effect of repumper laser addressing $F = 1 \rightarrow 1$ transition. (b) Temperature vs power of the repumper laser when $\Delta_{1 \rightarrow 1}/2\pi = +17.4$ MHz (filled blue circle) and -5.2 MHz (unfilled red circle). (c) Temperature vs detuning of the repumper laser when $P_{1 \rightarrow 1} = 10$ mW (unfilled green diamond), 20 mW (filled yellow triangle) and 31.5 mW (filled blue circle).

We fix the parameters to load the red detuned blue MOT at 26 mW power and -2.5 MHz detuned from the $5S_{1/2}$, $F = 2 \rightarrow 6P_{3/2}$, $F = 2$ transition. We then demonstrate the blue detuned blue MOT using the same transition by transferring the atoms from the red detuned blue MOT. This is done by switching off the L_3 beams and switching on the L_4 beams. The quadruple magnetic field is also increased to 45 G/cm. We wait for 20 ms for the atoms to settle in the blue detuned blue MOT. First, we vary the power of the blue detuned blue beam ($P_{2 \rightarrow 2}$) from 7 mW to 15 mW at $\Delta_{2 \rightarrow 2}/2\pi = +4$ MHz and observe that T decreases from 43 μK to 31 μK and saturates, as shown in Fig. 4 (c). We also reduced the blue detuned blue beam size by 4 times to confirm if we are limited by its power and observe no change in temperature at maximum available power.

Next we study the effect of the detuning of the blue detuned blue beam ($\Delta_{2 \rightarrow 2}$) at fixed power, $P_{2 \rightarrow 2} = 15$ mW. As the $\Delta_{2 \rightarrow 2}/2\pi$ is changed from +13 MHz to +5 MHz, T decreases from 90 μK to 31 μK and then further increases to > 40 μK as the frequency is changed towards resonance. We do not see any significant difference in temperature between the red detuned blue MOT and the

TABLE I. Temperature of the different MOTs. Detuning (Δ) of each laser from its corresponding transition is shown. IR repumper laser is driving the $5S_{1/2}$, $F = 1 \rightarrow 5P_{3/2}$, $F = X$ transition, where $X = 1$ or 2. Blue MOT laser is driving the $5S_{1/2}$, $F = 2 \rightarrow 6P_{3/2(1/2)}$, $F = X$ transition for the $D_{2(1)}$ MOT, where $X = 1, 2$ or 3.

IR Repumper	Blue MOT	T (μK)	
Transition Δ (MHz)	Transition Δ (MHz)		
1 \rightarrow 2	D ₂ , 2 \rightarrow 3	-3	65 \pm 2
1 \rightarrow 1	D ₂ , 2 \rightarrow 3	-3	44 \pm 2
1 \rightarrow 1	D ₂ , 2 \rightarrow 3	+2	53 \pm 2
1 \rightarrow 1	D ₂ , 2 \rightarrow 2	-2.5	32 \pm 1
1 \rightarrow 1	D ₂ , 2 \rightarrow 2	+5	31 \pm 1
1 \rightarrow 1	D ₁ , 2 \rightarrow 2	-2	40 \pm 1
1 \rightarrow 1	D ₁ , 2 \rightarrow 2	+5	24 \pm 1
1 \rightarrow 1	D ₁ , 2 \rightarrow 1	-2	61 \pm 2

blue detuned blue MOT with $5S_{1/2}$, $F = 2 \rightarrow 6P_{3/2}$, $F = 2$ transition.

We then carry out the same study for the blue MOT in the D₁ line at $5S_{1/2}$, $F = 2 \rightarrow 6P_{1/2}$, $F = 2$ transition, which is also a type-II open transition but of weaker tran-

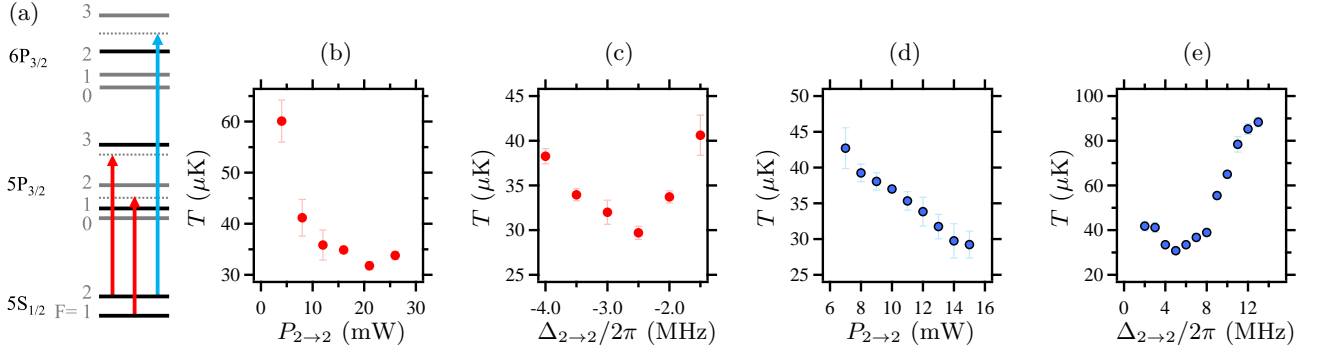


FIG. 4. (Color online) (a) Relevant energy levels for studying the effect of the blue laser addressing $F = 2 \rightarrow 2$ transition. (b) Temperature vs power of the 420 nm laser (L_3) when $\Delta_{2 \rightarrow 2}/2\pi = -2$ MHz. (c) Temperature vs detuning of the 420 nm laser (L_3) when $P_{2 \rightarrow 2} = 26$ mW. (d) Temperature vs power of the 420 nm blue detuned laser (L_4) when $\Delta_{2 \rightarrow 2}/2\pi = +5$ MHz. (e) Temperature vs detuning of the 420 nm blue detuned laser (L_4) when $P_{2 \rightarrow 2} = 15$ mW. In (b)-(e), $\Delta_{1 \rightarrow 1}/2\pi = +14$ MHz and $P_{1 \rightarrow 1} = 30$ mW.

sition strength as compared to the D_2 line. We observe that the minimum temperature of the red detuned blue MOT at D_1 line is $40 \mu\text{K}$. We then transfer the atoms to the blue detuned blue MOT at same line and observe that T is lowered to $24 \mu\text{K}$. No. of atoms in the blue detuned blue MOT at D_1 transition also decreases to 5×10^7 .

We also study other configurations of the blue MOT and minimum temperature achieved at different configurations are summarized in Table I. Unlike in [15], we have observed almost spherical shape of the atomic cloud with gaussian distribution of atoms in all different configurations of the MOTs.

V. CONCLUSION

In summary, we observe that SGC plays a crucial role in laser cooling in the sub-Doppler regime. Prior to this work, it was known that there is no sub-Doppler cooling with blue-detuned lasers in type-I transition. In this work, we show that it is possible to achieve cooling with blue-detuned lasers but in the absence of SGC. As SGC is fragile to stray magnetic fields, we observe blue-detuned cooling even in type-I transition in MOT. For completeness, we also explore various combinations for the effectiveness of blue-detuned laser cooling in both type-I and type-II MOT configurations, achieving temperatures as low as $24 \mu\text{K}$ in the D_1 MOT and $31 \mu\text{K}$ in the D_2 MOT.

ACKNOWLEDGMENTS

The authors are grateful to Prof. T. N. Dey for fruitful discussions. RCD acknowledges the Ministry of Education, Government of India, for the Prime Minister's Research Fellowship (PMRF), and K.P. acknowledges funding from DST through Grant No. DST/ICPS/QuST/Theme-3/2019.

APPENDIX

1. $F = 1 \rightarrow 2$ system

The remaining equations obtained using Density matrix analysis for the 8 level system are presented below.

$$\begin{aligned}
\dot{\rho}_{11} &= -\frac{i}{2}\Omega(\rho_{41} + \frac{1}{\sqrt{6}}\rho_{61}) + c.c. + \Gamma(\rho_{44} + \frac{1}{2}\rho_{55} + \frac{1}{6}\rho_{66}) \\
\dot{\rho}_{22} &= -\frac{i}{2\sqrt{2}}\Omega(\rho_{52} + \rho_{72}) + c.c. + \Gamma(\frac{1}{2}\rho_{55} + \frac{2}{3}\rho_{66} + \frac{1}{2}\rho_{77}) \\
\dot{\rho}_{33} &= -\frac{i}{2}\Omega(\frac{1}{\sqrt{6}}\rho_{63} + \rho_{83}) + c.c. + \Gamma(\frac{1}{6}\rho_{66} + \frac{1}{2}\rho_{77} + \rho_{88}) \\
\dot{\rho}_{44} &= \frac{i}{2}\Omega\rho_{41} + c.c. - \Gamma\rho_{44} \\
\dot{\rho}_{55} &= \frac{i}{2\sqrt{2}}\Omega\rho_{52} + c.c. - \Gamma\rho_{55} \\
\dot{\rho}_{66} &= \frac{i}{2\sqrt{6}}\Omega(\rho_{61} + \rho_{63}) + c.c. - \Gamma\rho_{66} \\
\dot{\rho}_{77} &= \frac{i}{2\sqrt{2}}\Omega\rho_{72} + c.c. - \Gamma\rho_{77} \\
\dot{\rho}_{88} &= \frac{i}{2\sqrt{2}}\Omega\rho_{83} + c.c. - \Gamma\rho_{88} \\
\dot{\rho}_{14} &= \frac{i}{2}\Omega(\rho_{11} - \rho_{44} - \frac{1}{\sqrt{6}}\rho_{64}) - i(\Delta - kv)\rho_{14} - \frac{1}{2}\Gamma\rho_{14} \\
\dot{\rho}_{15} &= \frac{i}{2}\Omega(\frac{1}{\sqrt{2}}\rho_{12} - \rho_{45} - \frac{1}{\sqrt{6}}\rho_{65}) - i(\Delta - kv)\rho_{15} - \frac{1}{2}\Gamma\rho_{15} \\
\dot{\rho}_{16} &= \frac{i}{2}\Omega(\frac{1}{\sqrt{6}}\rho_{11} + \frac{1}{\sqrt{6}}\rho_{13} - \rho_{46} - \frac{1}{\sqrt{6}}\rho_{66}) - i(\Delta + kv)\rho_{16} - \frac{1}{2}\Gamma\rho_{16} \\
\dot{\rho}_{17} &= \frac{i}{2}\Omega(\frac{1}{\sqrt{2}}\rho_{12} - \rho_{47} - \frac{1}{\sqrt{6}}\rho_{67}) - i(\Delta + kv)\rho_{17} - \frac{1}{2}\Gamma\rho_{17} \\
\dot{\rho}_{18} &= \frac{i}{2}\Omega(\rho_{13} - \rho_{48} - \frac{1}{\sqrt{6}}\rho_{68}) - i(\Delta + 3kv)\rho_{18} - \frac{1}{2}\Gamma\rho_{18} \\
\dot{\rho}_{24} &= \frac{i}{2}\Omega(\rho_{21} - \frac{1}{\sqrt{2}}\rho_{54} - \frac{1}{\sqrt{2}}\rho_{74}) - i(\Delta - kv)\rho_{24} - \frac{1}{2}\Gamma\rho_{24} \\
\dot{\rho}_{25} &= \frac{i}{2\sqrt{2}}\Omega(\rho_{22} - \rho_{55} - \rho_{75}) - i(\Delta - kv)\rho_{25} - \frac{1}{2}\Gamma\rho_{25} \\
\dot{\rho}_{26} &= \frac{i}{2}\Omega(\frac{1}{\sqrt{6}}\rho_{21} + \frac{1}{\sqrt{6}}\rho_{23} - \frac{1}{\sqrt{2}}\rho_{56} - \frac{1}{\sqrt{2}}\rho_{76}) - i(\Delta + kv)\rho_{26} - \frac{1}{2}\Gamma\rho_{26} \\
\dot{\rho}_{27} &= \frac{i}{2\sqrt{2}}\Omega(\rho_{22} - \rho_{57} - \rho_{77}) - i(\Delta + kv)\rho_{27} - \frac{1}{2}\Gamma\rho_{27} \\
\dot{\rho}_{28} &= \frac{i}{2}\Omega(\rho_{23} - \frac{1}{\sqrt{2}}\rho_{58} - \frac{1}{\sqrt{2}}\rho_{78}) - i(\Delta + 3kv)\rho_{28} - \frac{1}{2}\Gamma\rho_{28} \\
\dot{\rho}_{34} &= \frac{i}{2}\Omega(\rho_{31} - \frac{1}{\sqrt{6}}\rho_{64} - \rho_{84}) - i(\Delta + kv)\rho_{34} - \frac{1}{2}\Gamma\rho_{34} \\
\dot{\rho}_{35} &= \frac{i}{2}\Omega(\frac{1}{\sqrt{2}}\rho_{32} - \frac{1}{\sqrt{6}}\rho_{65} + \rho_{85}) - i(\Delta + kv)\rho_{35} - \frac{1}{2}\Gamma\rho_{35} \\
\dot{\rho}_{36} &= \frac{i}{2}\Omega(\frac{1}{\sqrt{6}}\rho_{31} + \frac{1}{\sqrt{2}}\rho_{33} - \frac{1}{\sqrt{6}}\rho_{66} - \rho_{86}) - i(\Delta + 3kv)\rho_{36} - \frac{1}{2}\Gamma\rho_{36} \\
\dot{\rho}_{37} &= \frac{i}{2}\Omega(\frac{1}{\sqrt{2}}\rho_{32} - \frac{1}{\sqrt{6}}\rho_{67} - \rho_{87}) - i(\Delta + 3kv)\rho_{37} - \frac{1}{2}\Gamma\rho_{37}
\end{aligned}$$

$$\begin{aligned}
\dot{\rho}_{38} &= \frac{i}{2}\Omega(\rho_{33} - \frac{1}{\sqrt{6}}\rho_{68} - \rho_{88}) - i(\Delta + 5kv)\rho_{38} - \frac{1}{2}\Gamma\rho_{38} \\
\dot{\rho}_{45} &= \frac{i}{2\sqrt{2}}\Omega\rho_{42} - \frac{i}{2}\Omega^*\rho_{15} - \Gamma\rho_{45} \\
\dot{\rho}_{46} &= \frac{i}{2\sqrt{6}}\Omega(\rho_{41} + \rho_{43}) - \frac{i}{2}\Omega^*\rho_{16} - 2ikv\rho_{46} - \Gamma\rho_{46} \\
\dot{\rho}_{47} &= \frac{i}{2\sqrt{2}}\Omega\rho_{42} - \frac{i}{2}\Omega^*\rho_{17} - 2ikv\rho_{47} - \Gamma\rho_{47} \\
\dot{\rho}_{48} &= \frac{i}{2}\Omega\rho_{43} - \frac{i}{2}\Omega^*\rho_{18} - 4ikv\rho_{48} - \Gamma\rho_{48} \\
\dot{\rho}_{56} &= \frac{i}{2\sqrt{6}}\Omega(\rho_{51} + \rho_{53}) - \frac{i}{2\sqrt{2}}\Omega^*\rho_{26} - 2ikv\rho_{56} - \Gamma\rho_{56}
\end{aligned}$$

$$\begin{aligned}
\dot{\rho}_{57} &= \frac{i}{2\sqrt{2}}\Omega(\rho_{52} - \rho_{27}) - 2ikv\rho_{57} - \Gamma\rho_{57} \\
\dot{\rho}_{58} &= \frac{i}{2}\Omega(\rho_{53} - \frac{1}{\sqrt{2}}\rho_{28}) - 4ikv\rho_{58} - \Gamma\rho_{58} \\
\dot{\rho}_{67} &= \frac{i}{2\sqrt{2}}\Omega\rho_{62} - \frac{i}{2\sqrt{6}}\Omega^*(\rho_{37} + \rho_{17}) - \Gamma\rho_{67} \\
\dot{\rho}_{68} &= \frac{i}{2}\Omega\rho_{63} - \frac{i}{2\sqrt{6}}\Omega^*(\rho_{38} + \rho_{18}) - 2ikv\rho_{68} - \Gamma\rho_{68} \\
\dot{\rho}_{78} &= \frac{i}{2}\Omega\rho_{73} - \frac{i}{2\sqrt{2}}\Omega^*\rho_{28} - 2ikv\rho_{78} - \Gamma\rho_{78}
\end{aligned}$$

-
- [1] S. Menon and G. S. Agarwal, Effects of spontaneously generated coherence on the pump-probe response of a Λ system, *Phys. Rev. A* **57**, 4014 (1998).
- [2] A. Lezama, S. Barreiro, and A. M. Akulshin, Electromagnetically induced absorption, *Phys. Rev. A* **59**, 4732 (1999).
- [3] A. V. Taichenachev, A. M. Tumaikin, and V. I. Yudin, Electromagnetically induced absorption in a four-state system, *Phys. Rev. A* **61**, 011802 (1999).
- [4] W.-H. Xu, J.-H. Wu, and J.-Y. Gao, Transient response in a three-level v system with spontaneously generated coherence, *Optics Communications* **215**, 345 (2003).
- [5] E. Paspalakis, S.-Q. Gong, and P. L. Knight, Spontaneous emission-induced coherent effects in absorption and dispersion of a v -type three-level atom, *Optics Communications* **152**, 293 (1998).
- [6] D. Wang and Y. Zheng, Quantum interference in a four-level system of a ^{87}Rb atom: Effects of spontaneously generated coherence, *Phys. Rev. A* **83**, 013810 (2011).
- [7] Z. Song, Y. Peng, Z.-D. Sun, and Y. Zheng, Spontaneously generated coherence in a rb atom via photon counting statistics, *Journal of Physics B: Atomic, Molecular and Optical Physics* **49**, 015001 (2015).
- [8] A. Silatan, M. Ghaderi GoranAbad, and M. Mahmoudi, Optical limiting via spontaneously generated coherence, *Scientific Reports* **13**, 364 (2023).
- [9] J. A. Devlin and M. R. Tarbutt, Three-dimensional doppler, polarization-gradient, and magneto-optical forces for atoms and molecules with dark states, *New Journal of Physics* **18**, 123017 (2016).
- [10] J. P. McGilligan, P. F. Griffin, R. Elvin, S. J. Ingleby, E. Riis, and A. S. Arnold, Grating chips for quantum technologies, *Scientific Reports* **7**, 384 (2017).
- [11] Y.-S. Chin, M. Steiner, and C. Kurtsiefer, Polarization gradient cooling of single atoms in optical dipole traps, *Phys. Rev. A* **96**, 033406 (2017).
- [12] M. Walhout, U. Sterr, and S. L. Rolston, Magnetic inhibition of polarization-gradient laser cooling in $\sigma_+ - \sigma_-$ optical molasses, *Phys. Rev. A* **54**, 2275 (1996).
- [13] M. Walhout, J. Dalibard, S. L. Rolston, and W. D. Phillips, $\sigma_+ - \sigma_-$ optical molasses in a longitudinal magnetic field, *J. Opt. Soc. Am. B* **9**, 1997 (1992).
- [14] K. N. Jarvis, J. A. Devlin, T. E. Wall, B. E. Sauer, and M. R. Tarbutt, Blue-detuned magneto-optical trap, *Phys. Rev. Lett.* **120**, 083201 (2018).
- [15] K. N. Jarvis, B. E. Sauer, and M. R. Tarbutt, Characteristics of unconventional rb magneto-optical traps, *Phys. Rev. A* **98**, 043432 (2018).
- [16] B. Piest, V. Vollenkemper, J. Böhm, A. Herbst, and E. M. Rasel, Red- and blue-detuned magneto-optical trapping with liquid crystal variable retarders, *Review of Scientific Instruments* **93**, 023202 (2022).
- [17] J. J. Bureau, P. Aggarwal, K. Mehling, and J. Ye, Blue-detuned magneto-optical trap of molecules, *Phys. Rev. Lett.* **130**, 193401 (2023).
- [18] S. Xu, R. Li, Y. Xia, M. Siercke, and S. Ospelkaus, Blue-detuned molecular magneto-optical trap schemes based on bayesian optimization, *Phys. Rev. A* **108**, 033102 (2023).
- [19] V. Jorapur, T. K. Langin, Q. Wang, G. Zheng, and D. DeMille, High density loading and collisional loss of laser cooled molecules in an optical trap (2023), [arXiv:2307.05347 \[physics.atom-ph\]](https://arxiv.org/abs/2307.05347).
- [20] S. J. Li, C. M. Holland, Y. Lu, and L. W. Cheuk, A blue-detuned magneto-optical trap of caf molecules (2023), [arXiv:2311.05447 \[physics.atom-ph\]](https://arxiv.org/abs/2311.05447).
- [21] R. C. Das, D. Shylla, A. Bera, and K. Pandey, Narrow-line cooling of ^{87}rb using $5s_{1/2} \rightarrow 6p_{3/2}$ open transition at 420 nm, *Journal of Physics B: Atomic, Molecular and Optical Physics* **56**, 025301 (2023).
- [22] R. Ding, A. Orozco, J. Lee, and N. Claussen, *Narrow-linewidth laser cooling for rapid production of low-temperature atoms for high data-rate quantum sensing.*, Tech. Rep. (Sandia National Lab.(SNL-NM), Albuquerque, NM (United States), 2022).
- [23] R. C. Das, S. Khan, T. R, and K. Pandey, Continuous loading of magneto-optical trap of rb at narrow transition (2024), [arXiv:2401.08286 \[physics.atom-ph\]](https://arxiv.org/abs/2401.08286).
- [24] P. M. Duarte, R. A. Hart, J. M. Hitchcock, T. A. Corcovilos, T.-L. Yang, A. Reed, and R. G. Hulet, All-optical production of a lithium quantum gas using narrow-line laser cooling, *Phys. Rev. A* **84**, 061406 (2011).
- [25] J. Sebastian, C. Gross, K. Li, H. C. J. Gan, W. Li, and K. Dieckmann, Two-stage magneto-optical trapping and narrow-line cooling of ^6li atoms to high phase-space density, *Phys. Rev. A* **90**, 033417 (2014).
- [26] D. C. McKay, D. Jervis, D. J. Fine, J. W. Simpson-Porco, G. J. A. Edge, and J. H. Thywissen, Low-temperature high-density magneto-optical trapping of potassium using the open $4s \rightarrow 5p$ transition at 405 nm, *Phys. Rev. A* **84**, 063420 (2011).
- [27] E. A. Curtis, C. W. Oates, and L. Hollberg, Quenched narrow-line laser cooling of ^{40}ca to near the photon recoil limit, *Phys. Rev. A* **64**, 031403 (2001).
- [28] E. A. Curtis, C. W. Oates, and L. Hollberg, Quenched narrow-line second- and third-stage laser cooling of ^{40}ca , *J. Opt. Soc. Am. B* **20**, 977 (2003).
- [29] H. Katori, T. Ido, Y. Isoya, and M. Kuwata-Gonokami, Magneto-optical trapping and cooling of strontium atoms down to the photon recoil temperature, *Phys. Rev. Lett.* **82**, 1116 (1999).
- [30] T. Yang, K. Pandey, M. S. Pramod, F. Leroux, C. C. Kwong, E. Hajiyev, Z. Y. Chia, B. Fang, and D. Wilkowski, A high flux source of cold strontium atoms,

- The European Physical Journal D **69**, 226 (2015).
- [31] T. Kuwamoto, K. Honda, Y. Takahashi, and T. Yabuzaki, Magneto-optical trapping of yb atoms using an intercombination transition, *Phys. Rev. A* **60**, R745 (1999).
- [32] K. Pandey, K. D. Rathod, A. K. Singh, and V. Natarajan, Atomic fountain of laser-cooled yb atoms for precision measurements, *Phys. Rev. A* **82**, 043429 (2010).
- [33] M. Lu, S. H. Youn, and B. L. Lev, Spectroscopy of a narrow-line laser-cooling transition in atomic dysprosium, *Phys. Rev. A* **83**, 012510 (2011).
- [34] T. Maier, H. Kadau, M. Schmitt, A. Griesmaier, and T. Pfau, Narrow-line magneto-optical trap for dysprosium atoms, *Opt. Lett.* **39**, 3138 (2014).
- [35] A. J. Berglund, J. L. Hanssen, and J. J. McClelland, Narrow-line magneto-optical cooling and trapping of strongly magnetic atoms, *Phys. Rev. Lett.* **100**, 113002 (2008).
- [36] A. Frisch, K. Aikawa, M. Mark, A. Rietzler, J. Schindler, E. Zupanič, R. Grimm, and F. Ferlaino, Narrow-line magneto-optical trap for erbium, *Phys. Rev. A* **85**, 051401 (2012).
- [37] B. Seo, P. Chen, Z. Chen, W. Yuan, M. Huang, S. Du, and G.-B. Jo, Efficient production of a narrow-line erbium magneto-optical trap with two-stage slowing, *Phys. Rev. A* **102**, 013319 (2020).
- [38] A. Yamaguchi, M. S. Safronova, K. Gibble, and H. Katori, Narrow-line cooling and determination of the magic wavelength of cd, *Phys. Rev. Lett.* **123**, 113201 (2019).
- [39] Y. Miyazawa, R. Inoue, H. Matsui, K. Takanashi, and M. Kozuma, Narrow-line magneto-optical trap for europium, *Phys. Rev. A* **103**, 053122 (2021).
- [40] J. Dalibard and C. Cohen-Tannoudji, Laser cooling below the doppler limit by polarization gradients: simple theoretical models, *J. Opt. Soc. Am. B* **6**, 2023 (1989).
- [41] S. Chang and V. Minogin, Density-matrix approach to dynamics of multilevel atoms in laser fields, *Physics Reports* **365**, 65 (2002).
- [42] R. C. Das, S. Khan, T. R., and K. Pandey, Direct spectroscopy of rubidium using a narrow-line transition at 420 nm (2024), [arXiv:2401.13350](https://arxiv.org/abs/2401.13350) [physics.atom-ph].